Consistent modelling of a single PEM fuel cell using Onsager's principle.

L. Valiño,[1,], R. Mustata, L. Dueñas

LIFTEC-CSIC, Universidad de Zaragoza, María de Luna 10, 50018-Zaragoza, Spain

Abstract

In this paper a novel approach for three-dimensional (3D) modelling is proposed for a High Temperature Exchange Membrane Fuel Cell (HTPEMFC). This new modelling is based on Onsager's principle of minimum energy dissipation that is applicable for near equilibrium and coupled irreversible systems. In particular, for low conductivity membranes, this leads to a one directional proton movement through the membrane. The resulting equations are numerically solved for a real single cell geometry, using a 3D finite volume discretization. Results are analyzed and validated against experimental data.

Keywords: PEMFC, current density, hydrogen, polarization curve.

Email addresses: valino@litec.csic.es (L. Valiño,), radu@litec.csic.es (R. Mustata), leoduenas@litec.csic.es (L. Dueñas)

1. Introduction

Fuel cells are nowadays extensively studied due to their potential as an alternative energy converter for a wide range of applications. They have unique technological attributes: efficiency, absence of moving parts and very low emissions. In particular, the proton-exchange membrane fuel cells (PEMFC) are today in the focus of interest as one of the most promising technologies in development for the automotive industry and stationary power plants.

Numerical calculations are a very valuable engineering tool which could be applied to obtain hints for the development of optimal control and operating strategies of these devices. Consequently, there is a need to simulate the internal processes (reactions, mass transport, heat transport) occurring in a fuel cell, which in its turn requires a formulation of adequate physical models. Besides, many of the physical phenomena taking place in a fuel cell, such as the electrochemical reactions, mass and heat transport, canot be observed directly in experiments, at least not in significant zones of the cell. A better understanding of these highly coupled processes could then be obtained by the use of good physical models and numerical methods.

In the past couple of decades a large number of modelling strategies have been adopted, starting with the one-dimensional models of Springer et al. [1] and Bernardi and Verbrugge [2, 3]. Several two-dimensional models have been presented by researchers [4], [5] and [6]. Most of these models compute the flow field along a single channel to study the reaction species and current density distributions. Results of polarization curves are well correlated with experimental data.

Three-dimensional (3D) models account for the effect of the complex geometry and allow a parametric study for a realistic flow field, concentration and current distributions. Works including these models have been published since the last nineties (Shimpalee et al. [7]). Berning et al. [8] developed a 3D PEMFC model including irreversibilities and entropic heat terms at catalyst layers, and Joule heating at the membrane. Zhou and Liu [9] developed a three-dimensional PEMFC model, ignoring the reversible reaction heat (entropic heat of reactions). Recent publications consider special aspects of the fuel cell operation, as cold-start [10], gas-feeding modes [11, 12], or temperature [13]. There is also an increasing interest in numerical aspects [14] or even new solver approaches [15]. PBI membranes have been also studied [16].

The present paper presents a 3D, steady state, constant density and isothermal electrochemical and species transport modeling for a PBI-based high temperature PEMFC (HTPEMFC). A new modelling approach is considered, which is based on the principle of least dissipation of energy (Onsager, see [17]) for coupled and near equilibrium "linear" systems. This linear description applies if the thermodynamic fluxes are linearly related to the thermodynamic forces, associated with minimum entropy production, thus the dissipation energy rate will be also minimal. In the case of low protonic conductivity membranes, the minimal disspation of energy leads to a practically one directional movement of protons through the membrane and the catalyst layers. This approach, phyisically sounded, allows for a great simplification in the numerical solution, which is shown in detail in section 4. The model couples various physical phenomena, electrochemical reactions and transport through porous media. In the first part, the mathematical equations describing the model are presented and also their coupling through an iterative numerical procedure. All the numerics are developed as modules/solvers of OpenFOAM, a free,

opensource finite volume with polyhedral mesh support code. The model is subsequently applied to a 3D configuration of an in-house developed single cell and the results are compared with the readily available experimental data, showing a high degree of agreement.

2. Model Description

Any mathematical model of a physical phenomena has to strike a balance between the level of complexity and the computational effot needed. The proposed PEM fuel cell model is a comprehensive 3D, isothermal, constant density and steady-state model with further assumptions:

- Infinitely thin catalyst layers
- Fick diffusion
- High temperature fuel cell (non liquid water)
- Hydrogen water vapor at anode inlet and oxygen and water vapor at cathodic inlet
- Butler-Vomer equations for electrochemical kinetics
- Migration of H^+ protons through the membrane obeying Onsager's principle

The equations governing these processes include the full mass and momentum conservation equations (Navier-Stokes), species transport, and additonal phenomenological equations specific to fuel cells. These equations, with appropriate boundary conditions, were implemented into their 3D form in a custom solver in OpenFOAM and an iterative numerical solution was developed in order to obtain and compare characteristic curves for an in-house prepared high temperature fuel cell with the simulation results.

The general idea is to consider the chemical reactions that take place at the catalytic layers, as outflow of the entire domain. The fuel cell will be divided in three regions, namely the anode with the gas diffusion layer (GDL) and the catalyst surface, the membrane and the cathode with its corresponding gas difussion layer and catalyst surface. The information between them will be given by the fluxes coupled at the boundaries as it will be explained in the following sections.

2.1. Fluid flow equations

In the channels of the bipolar plates, the 3D steady version of the incompressible Navier-Stokes equations is used, μ being the dynamic viscosity:

Continuity:

$$\frac{\partial u_j}{\partial x_j} = 0, \tag{1}$$

Momentum:

$$u_j \frac{\partial u_i}{\partial x_j} = -\frac{1}{\rho}\frac{\partial p}{\partial x_i} + \mu \frac{\partial^2 u_i}{\partial x_j \partial x_j}. \tag{2}$$

For the GDL, it is convenient to distinguish between two types of volume averages of the physical magnitudes of interest inside the porous media [18]:

Superficial average:

$$\langle \bullet \rangle = \frac{1}{V} \int_V \bullet \, \mathrm{dV}, \tag{3}$$

Intrinsic average:

$$\langle \bullet \rangle^\beta = \frac{1}{V_\beta} \int_{V_\beta} \bullet \, \mathrm{dV}_\beta, \tag{4}$$

where β indicates the zone available for the fluid inside the porous media (the "void" part in opposition to the solid part), and V indicates a small enough volume used to calculate the average. In agreement with the notation used, V_β indicates the void part inside the volume V, its fraction being the porosity ε by definition. Hence superficial and intrinsic averages are related through $\langle \bullet \rangle = \varepsilon \langle \bullet \rangle^\beta$.

It can be shown [18, 19] that under appropriate conditions, the superficial averaged velocity is the matching quantity to the flow velocity and that the intrinsic averaged pressure is the matching quantity to the flow pressure inside the porous media. This is used for simplifying the notation, so $\mathbf{u}$ and p will be directly written for equations inside the porous media. For a steady state approximation, the conservations equations are

Continuity inside GDL:

$$\frac{\partial u_j}{\partial x_j} = 0, \tag{5}$$

Momentum inside GDL:

$$\frac{1}{\varepsilon^2} u_j \frac{\partial u_i}{\partial x_j} = -\frac{1}{\rho} \frac{\partial p}{\partial x_i} + \frac{\nu}{\varepsilon} \frac{\partial^2 u_i}{\partial x_j \partial x_j} - \frac{\nu}{K} u_i, \tag{6}$$

where ε is the porosity and K is the permeability, assuming an isotropic and homogeneous porous medium. The second term on the right hand side of Equation 6 is known as the Brinkman approximation, and the third one reflects the contribution of Darcy's law. One can observe that Equations 1 and 2 are recovered in the case of porosity in the channels equal to unity and infinite permeability. Using simplifying assumptions [18, 19], Equations 5 and 6 can be used throughout the whole domain without the need of any "internal" boundary conditions.

2.2. Anode and Cathode

For the anodic "a" and cathodic "c" domain (channels+GDl+catalyst), the above explained equations, namely 5 and 6 will be solved for velocity and pressure fields, as well as a generic transport equation for the mass fraction of reactants $C \in \{C_{H_2}, C_{O_2}\}$, namely:

$$u_{sj} \frac{\partial C}{\partial x_j} = \frac{\partial}{\partial x_j} \gamma^s_{ef} \frac{\partial C}{\partial x_j}, \tag{7}$$

with $\gamma^s_{ef}, s \in \{a, c\}$ is the effective diffusion coefficient, depending on the porous media. According to [20],

$$\gamma^s_{ef} = \varepsilon \left(\frac{\varepsilon - \varepsilon_p}{1 - \varepsilon_p} \right)^\alpha \gamma \tag{8}$$

where γ is the diffusion coefficient in the free media, ε_p is the threshold porosity for filtering and α is a fitting parameter The water vapor mass fraction will be then calculated as the remaining part up to unity.

We use the approximation of an infinitely thin catalyst layer. This means that at the catalyst layer(s), the sum of diffusive and convective flow of reactants (hydrogen for anode and oxygen for cathode) balances out the mass flow (actually, its electrical equivalent) entering the membrane (hydrogen) or creating water (oxygen) due to the electrochemical reactions. This is expressed as a boundary condition at the catalyst layer(s). This and the remaining imposed boundary conditions are summarised in Table 1.

Anode		Cathode
	Walls:	
$\mathbf{u} = 0$		$\mathbf{u} = 0$
$\frac{\partial C_{O_2}}{\partial x_n} = 0$		$\frac{\partial C_{O_2}}{\partial x_n} = 0$
	Porous media walls: (free slip)	
$\mathbf{u} \cdot n = 0$		$\mathbf{u} \cdot n = 0$
	Inlet:	
ρu_a		ρu_c
C_{H_2}		C_{O_2}
	Free outlet:	
$\frac{\partial u_a}{\partial x_n} = 0$		$\frac{\partial u_c}{\partial x_n} = 0$
$\frac{\partial C_{H_2}}{\partial x_n} = 0$		$\frac{\partial C_{O_2}}{\partial x_n} = 0$
	Catalyst layer (outflow):	
ρu_a		ρu_c
$\rho u_a C_{H_2} - \rho \gamma^a_{ef} \frac{\partial C_{H_2}}{\partial x_n} = \rho u_a$		$\rho u_c C_{O_2} - \rho \gamma^c_{ef} \frac{\partial C_{O_2}}{\partial x_n} = 8 \rho u_c$

Table 1: Boundary conditions for the anode and cathode domains.

with pressure adjusting to velocity, that is to say zero gradient at all prescribed/calculated velocity boundaries and uniform zero elsewhere. The velocities expressed in the above boundary conditions are referred to their normal components.

3. Membrane

In principle, in the membrane, whatever its kind, a transport equation for the protons has to be solved. However, it is possible to avoid a full calculation by considering a significant (and poor) characteristic of today's polimeric membranes: their extremely low protonic conductivity. This implies that the dissipation due to the proton movement crossing through the membrane is very high. Hence, Onsager's principle of minimum disssipation can be applied. As mentioned above, Onsager's principle establishes that a system near the equilibrium forces its entropy generation to a minimum. As the membrane is so dissipative, this principle implies that the proton movement will be forced to be perpendicular to the catalyst layer, crossing the membrane by the shortest

path. The rest of the transported magnitudes in the cell will adapt to that. The consequence is that the proton movement is essentially one-dimensional, which greatly simplifies the protonic current calculation. In fact, for carrying out that calculation, the knowledge of the protonic conductivity suffices, as it will be next explained.

First, proper boundary, or rather, matching conditions have to be established at the catalyst layers-membrane interfaces. In this work, the catalyst layers, as mentioned above, will be taken as inifinetly thin surfaces. So, for the anode, we need to match the protonic current crossing the membrane with the hydrogen flux leaving their electrons at the catalyst layer. Hence, the mass flow of H_2 (equality (a) of Equation 9) has to be balanced with the protonic flux associated with the electrochemical reaction (equality (b) of Equation 9; Butler-Volmer equation). This equation reads:

$$j_a \overset{(a)}{=} \frac{\rho u_a 2F}{W_{H_2}} \overset{(b)}{=} j_{ar} \left(\frac{C_{H_2}}{C_{H_2 r}} \right)^{1/2} \left(\frac{\alpha_a + \alpha_c}{RT} F \eta_a \right), \tag{9}$$

where j_a is the (superficial) current density, F is the Faraday's constant, R is universal gas constant, T the operating temperature, j_{ar} is the reference current density, $\alpha_a,\ \alpha_c$ are the transfer coefficients and $C_{H_2 r}$ a reference mass fraction.

In the cathode side, where the oxygen mass flow, plus the external electronic current, has to match the protonic current to form water, the analogous equation reads:

$$j_c \overset{(a)}{=} \frac{\rho u_c 4F}{W_{O_2}} \overset{(b)}{=} j_{cr} \left(\frac{C_{O_2}}{C_{O_2 r}} \right) \exp\left(\frac{\alpha_c}{RT} F \eta_c \right), \tag{10}$$

Notice that $j_a \equiv j_a(x_2, x_3) \equiv j(x_1 = x_a, x_2, x_3$, where x_a is the anode catalyst layer location, is a 2 variable function, as, it is $j_c \equiv j_c(x_2, x_3) \equiv j(x_1 = x_c, x_2, x_3$, where x_c is the cathode catalyst layer location. This is also true for other functions defined at the catalyst layer(s) location and expressed with the subindex a or c, as the electronic and protonic potential.

Now, Onsager's principle implies that protons cross the membrane following a normal path. That is, the protonic current at a certain location at the membrane entry j_a should be equal to the protonic current j_c at its corresponding point at the cathode (the one with the same x_2 and x_3). Hence, the following equality holds:

$$j_a = j_c. \tag{11}$$

This also implies that the two corresponding anode-cathode points are related by Ohm's law. That is, if there is a protonic potential Φ_a^p at a certain location at the membrane entry, then its corresponding point at the cathode will have an electronic potential Φ_c^p such that:

$$\Phi_c^p = \Phi_a^p - \frac{L j_a}{\sigma}, \tag{12}$$

where L is the membrane thickness and σ the membrane conductivity. It is reminded that the electric potential difference is the driving force for the protons, whose interaction with the membrane generate heat losses, expressed through the inverse of the conductivity.

Notice that this principle can be applied to standard Nafion membranes too. There, as the local conductivity depends from the local level of hydration, liquid water transport should be considered (which will be essentially one-dimensional by Onsager's principle).

Finally note that there is one more implicit condition. It is supposed that the electronic conductivities at the anode and cathode side are so big that the electronic potential can be considered constant along each catalytist layer.

4. Iterative method

The previous coupled equations should be numerically solved through some iterative method. For a given operating intensity I, in order to obtain the corresponding potential loss between the anode and cathode, we employ the following iterative numerical procedure:

1. To initialize the iterative process, a given intensity I is given at the anode, which is supposed to be uniformly distributed for a starting. This implies that at the anode catalyst layer, the anodic current is $j_a = \frac{I}{Aa}$ where Aa is the active area of the catalyst layer.
   Then
   $$j_a \xrightarrow{\text{9(a)}} \rho u_a \xrightarrow{\text{5,6,7}} C_{H_2} \xrightarrow{\text{9(b)}} \eta_a = -\Phi_a^p \tag{13}$$
2. The last equality holds due to the nil value of electronic potential convention at the hidrogen anode. Which is taken constant along the anode by the high electronic conductivity. As explained above, the current at corresponding points on both sides of the membrane stays the same, so $j_a = j_c$, with the protonic potential Φ_c^p obtained from the ohmic loss reflected in Equation 12. With this information, the iterative process at the cathode can be started:
   $$\begin{aligned} j_c \xrightarrow{\text{10(a)}} \rho u_c \xrightarrow{\text{5,6,7}} C_{O_2} \xrightarrow{\text{10(b)}} \eta_c, \Phi_c^p \to \Phi_c^e \to \\ \langle \Phi_c^e \rangle \xrightarrow{\text{10(b)}} j_c^\star \xrightarrow{I=const} j_c \end{aligned} \tag{14}$$
   It is reminded that the electronic potential is constant in both electrodes (electronic conductivity is very high), which means that its averaging is required at the catalyst layer. However, this averaging of the electronic potential Φ_c^e does not ensure conservation of the total intesity I, therefore a rescaling of the recalculated $j_c^\star$ is needed in the last step of the iterative process at the cathode, so that
   $$I = \int_h k\, j_c^* \mathrm{d}y. \tag{15}$$
   With the new value of j_c, which is equal to j_a, we can go back to the anode and continue with the next iteration step. A value of k close to unity inidicates convergence.

Out of the above explained iterative process, in the case of convergence, one would readily obtain the value of the over-potentials (losses) needed for calculating the point in the polarization curve by substracting them from the equlibrium potential.

The potential losses are calculated with the following relations

$$\begin{aligned} Anode : \eta_a &= \Phi_a^e - \Phi_a^c \\ Cathode : \eta_c &= E_0 + \Phi_c^p - \Phi_c^e \end{aligned} \tag{16}$$

thus:

$$\Delta\Phi = \Phi_c^e - \Phi_a^e = E_o - \eta_a - \eta_c - (\Phi_a^p - \Phi_c^p) \tag{17}$$

which is the point of the polarization curve for a given demanded intensity.

These quantities are schematically presented in Figure 1

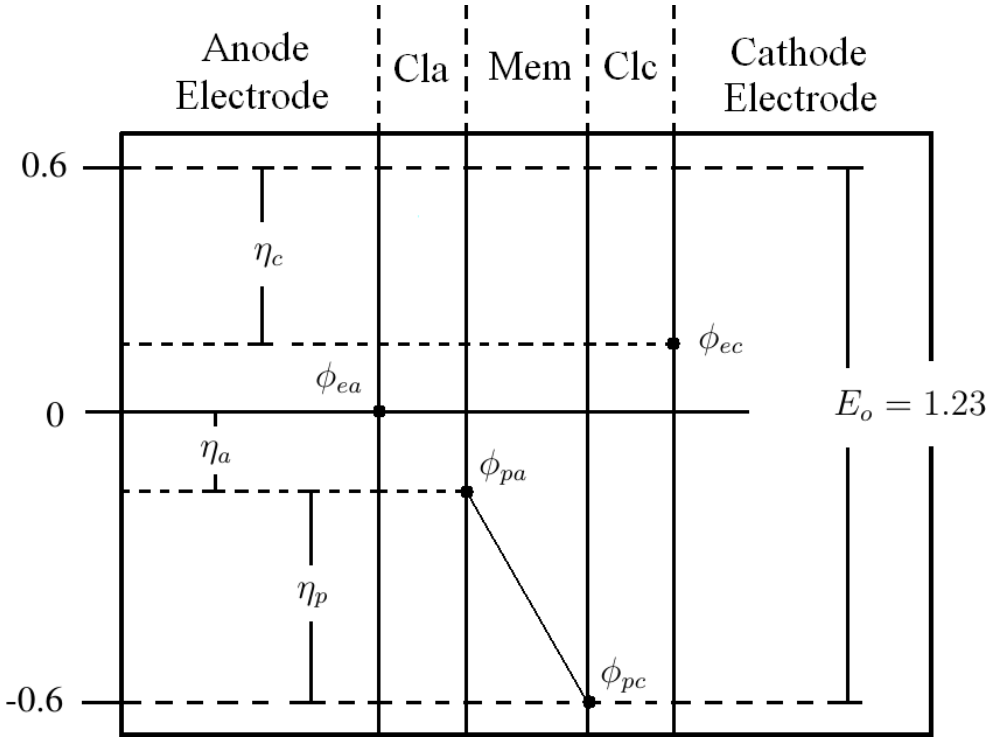

Figure 1: Potential loss diagram

5. Numerical Simulation and Results

The single cell that was tested in the in-house experimental facilities is illustrated in Figure 2.

The numerical study was performed on a $1M$ cells hexahedral mesh as presented in Figure 3 where the different components of the domain are also depicted (channels -zones 1 and 6-, GDL

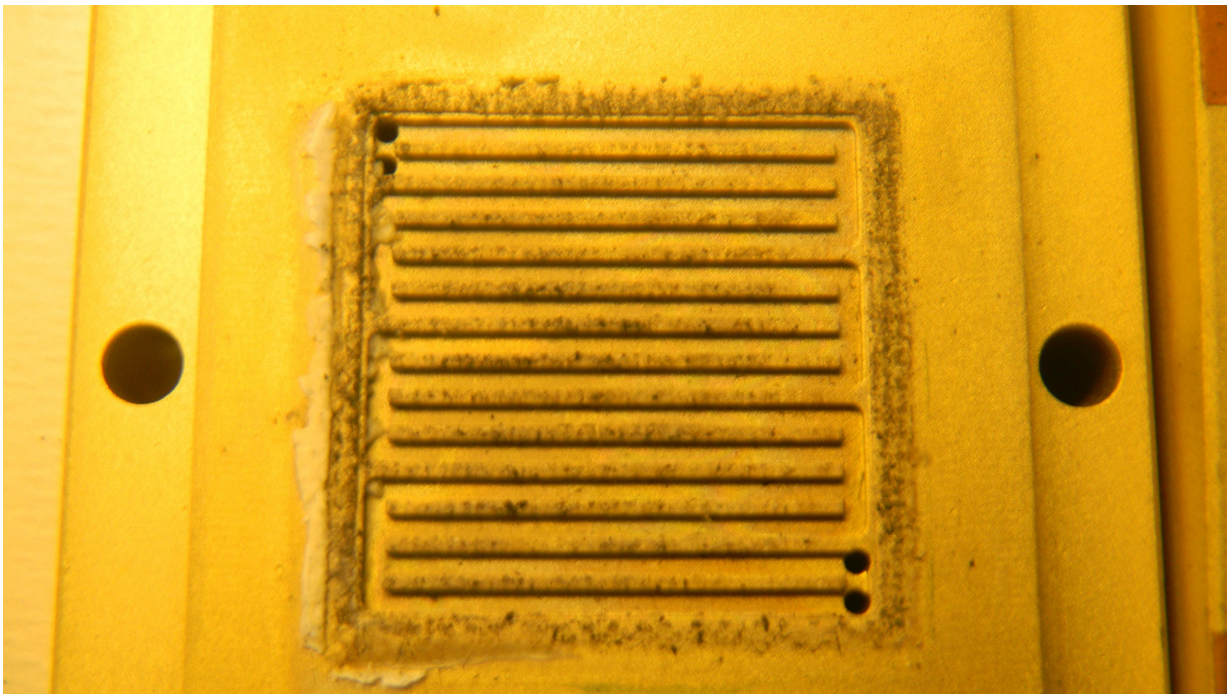

Figure 2: Studied single cell bipolar plate photo.

-zones 2 and 5- and catalyst layers -zone 3 and 4-), with the membrane omitted from calculations by virtue of our modelling approach)

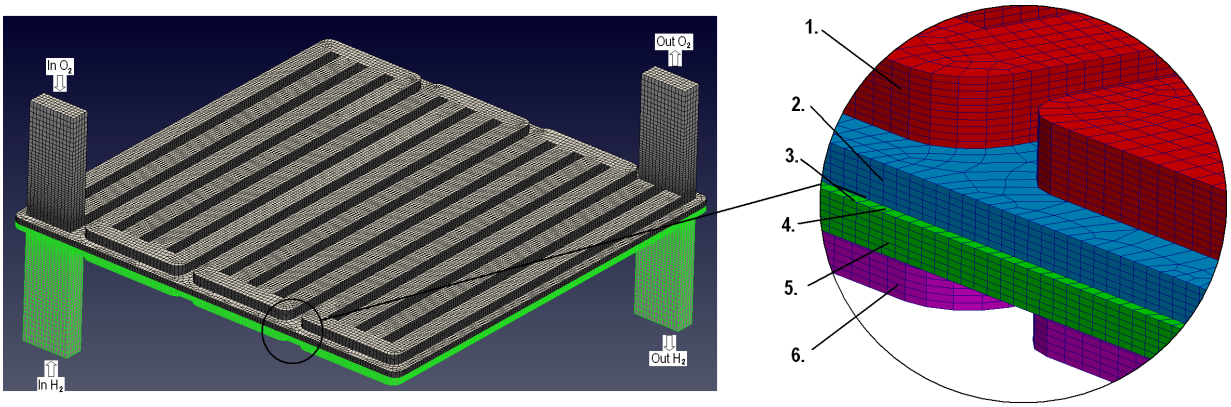

Figure 3: $1M$ cell mesh employed in the numerical simulation .

A BASF "Celtec®-P" high temperature membrane electron assembly (MEA) with an active area of 2×2 cm was used in a series of experiments at 120^o C. The physical parameters used for the the single cell numerical simulation are given in Table 2.

For the purpose of illustrating the behaviour of the fuel cell, an operating point of 2490A/m^2 was chosen. Figure 4 presents a zoom of the flux of gases in the cell. At the anode catalyst layer, the hidrogen flux corresponds to the protonic current, which is perpendicular as it is implied

Anode/Cathode gas diffusion layers thickness (m)	H	$2.9 \cdot 10^{-5}$
Anode/Cathode catalyst layer width (m)	W	10^{-5}
Membrane thickness (m)	L	$200 \cdot 10^{-6}$
Anode exchange current density (A/m^3)	J_{ar}	10^9
Cathode exchange current density (A/m^3)	J_{cr}	$2.5 \cdot 10^3$
Hydrogen reference mass fraction	$C_{H_{2r}}$	0.909657
Oxygen reference mass fraction	$C_{O_{2r}}$	1.09013
Anode transfer coefficient	α_a	1.32
Anode transfer coefficient	α_c	0.68
Faraday constant (Cul/mol)	F	96487
Universal gas constant $(J/(molKel))$	R	8.31472
H_2 reference molar concentration (Kg/mol)	M_{H_2}	$2 \cdot 10^{-3}$
O_2 reference molar concentration (Kg/mol)	M_{O_2}	0.032
Mixture H_2 density (Kg/m^3)	ρ_{H_2}	0.08988
Mixture O_2 density (Kg/m^3)	ρ_{O_2}	1.2
Temperature (K)	T	393
Porosity	ε	0.517
permeability (m^2)	K	$2.584 \cdot 10^{-13}$

Table 2: Physical parameters and properties.

by Onsager's principle. At the cathode catalyst layer, the oxygen flux only reflects a boundary condition related to electrochemistry.

Figure 5 presents the hydrogen and oxygen mass fractions. It can be observed that due to the progressive consumption of H_2 through the catalytic layer, its mass fraction diminishes as we move towards the exit of the channel from the bipolar plate. Also, higher concentrations of reactants are encountered at the catalyst layer areas that match the geometry of the bipolar plate channels.

Figure 6 shows the hydrogen mass fraction versus the cathode overpotential. The fact that is not uniform is due to the non-uniformity of the protonic overpotential, the electronic one being uniform as a consequence of the numerical algorithm with the assumption of infinite electronic conductivity at the catalyst layers.

In figure 7 the current density distribution is presented at the cathode side, distribution that is matched at the anode side due to the uni-directional mapping of the currents. As expected, the current density follows the pattern of the mass concentration of hydrogen. The effect is that local zones where the mass concentration is higher are reflected in higher current densities.

In figure 8, the spatial distribution of the anodic and cathodic overpotentials is showed. As expected, the cathodic overpotentail is orders of magnitude higher than the anodic one, with peaks in regions of low mass concentration of reactants, in our case towards the downstream end of the catalyst layers with respect to the flow through the bipolar plates channels.

It can be seen in this figure 9 the velocity vectors (fluid flow) coming into the anodic side and the exit vectors over the catalytic surface. The vectors are not scaled by their magnitude. It

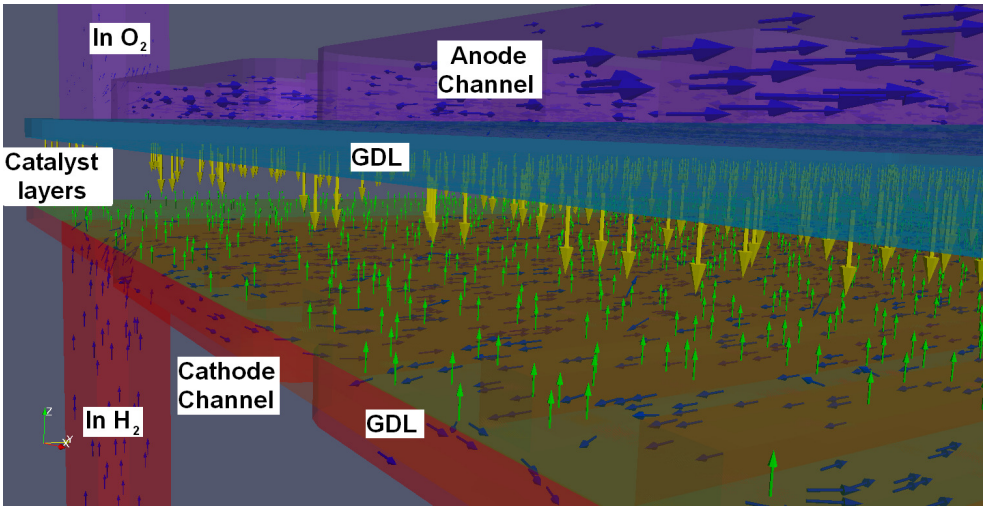

Figure 4: Detail of gas fluxes in the cell

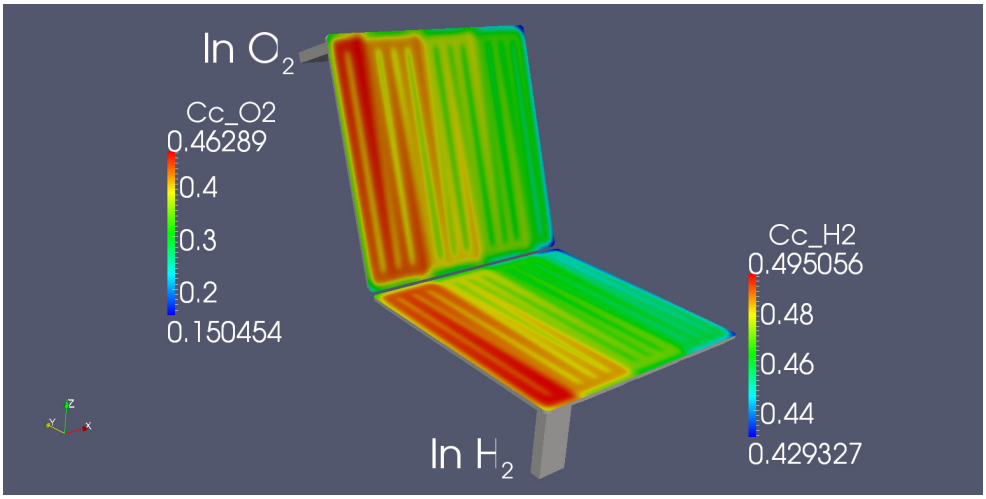

Figure 5: Hydrogen (horizontal) and Oxygen (rotated) mass fraction.

[1]

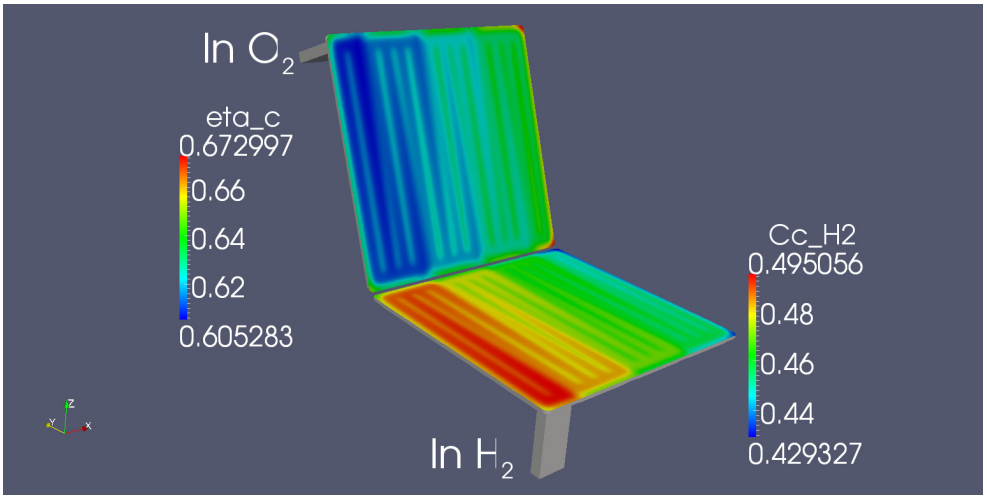

11

Figure 6: Anode mass fraction (horizontal) and Cathode overpotential (rotated).

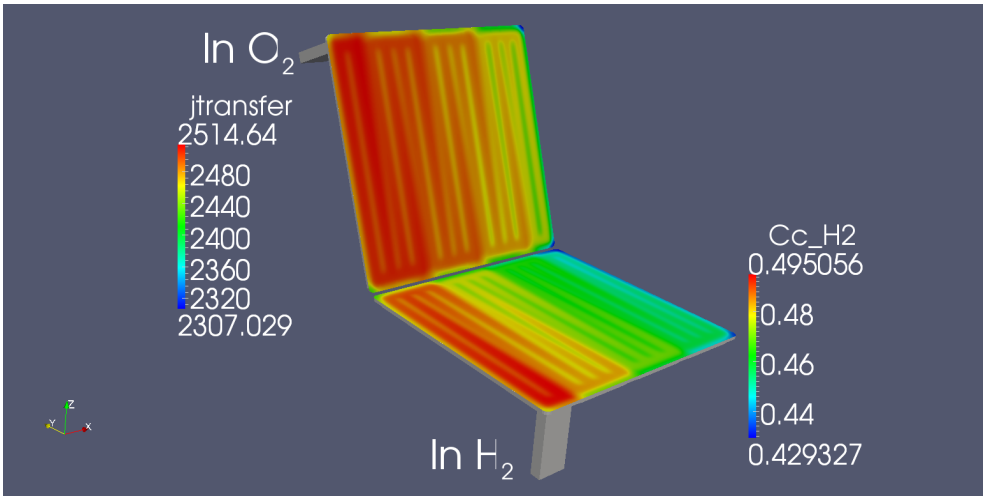

Figure 7: Anode mass fraction (horizontal) and Cathode current density (rotated).

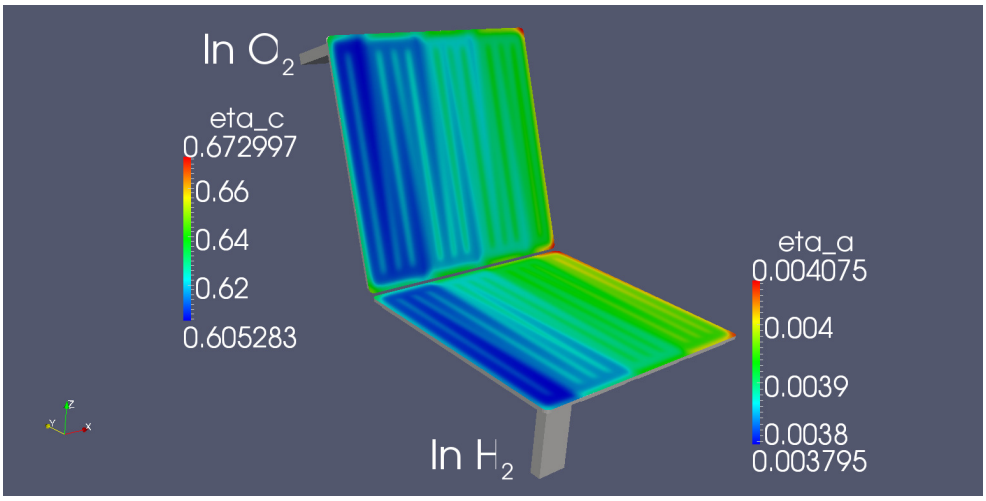

Figure 8: Anodic (horizontal) and cathodic (rotated) overpotentials.

can be observed the uni-directionality of the flow and also that is normal to the surface (catalytic surface).

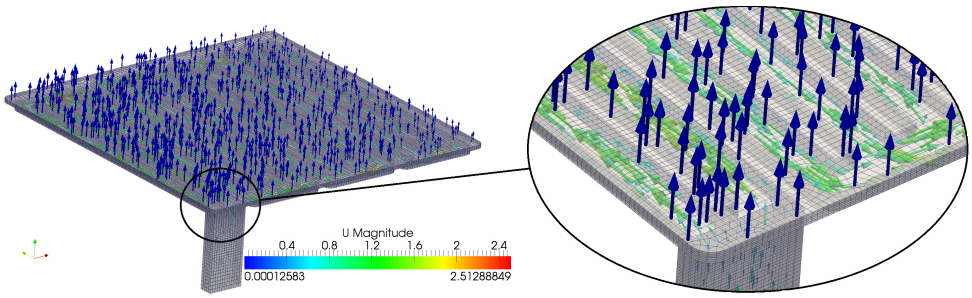

Figure 9: Velocity vectors.

The simulated polarization curve is depicted in figure 10, showing an excellent agreement with the experimental one.

The power density curve, shown in Figure 11, represents the power delivered by the single cell, which gives the range of values of current density at which the fuel cell could operate and deliver its maximum electric power. It can be observed that the results match very well with experimental data.

6. Conclusions

In this work, a 3D steady state, constant density and isothermal modeling for a PBI-based HTPEMFC has been presented and numerically solved, using the principle of least dissipation of energy (Onsager). This principle imposes a one-dimensional behaviour of the protonic current

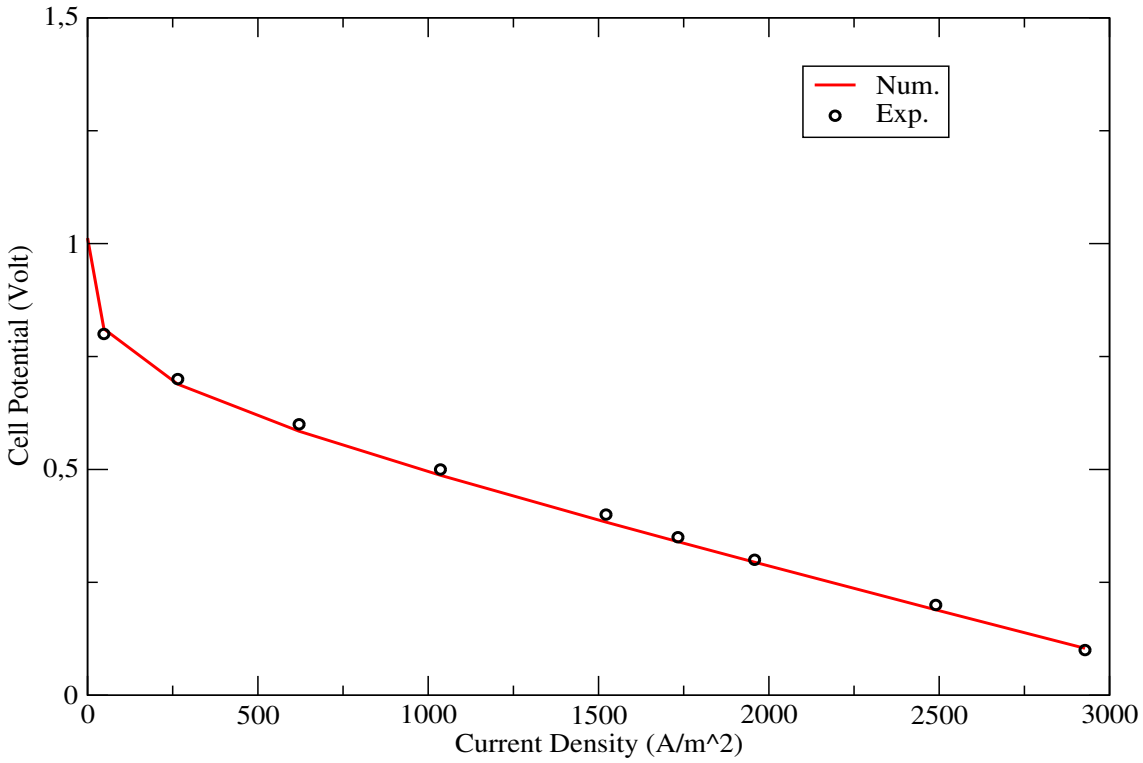

Figure 10: Polarization curve.

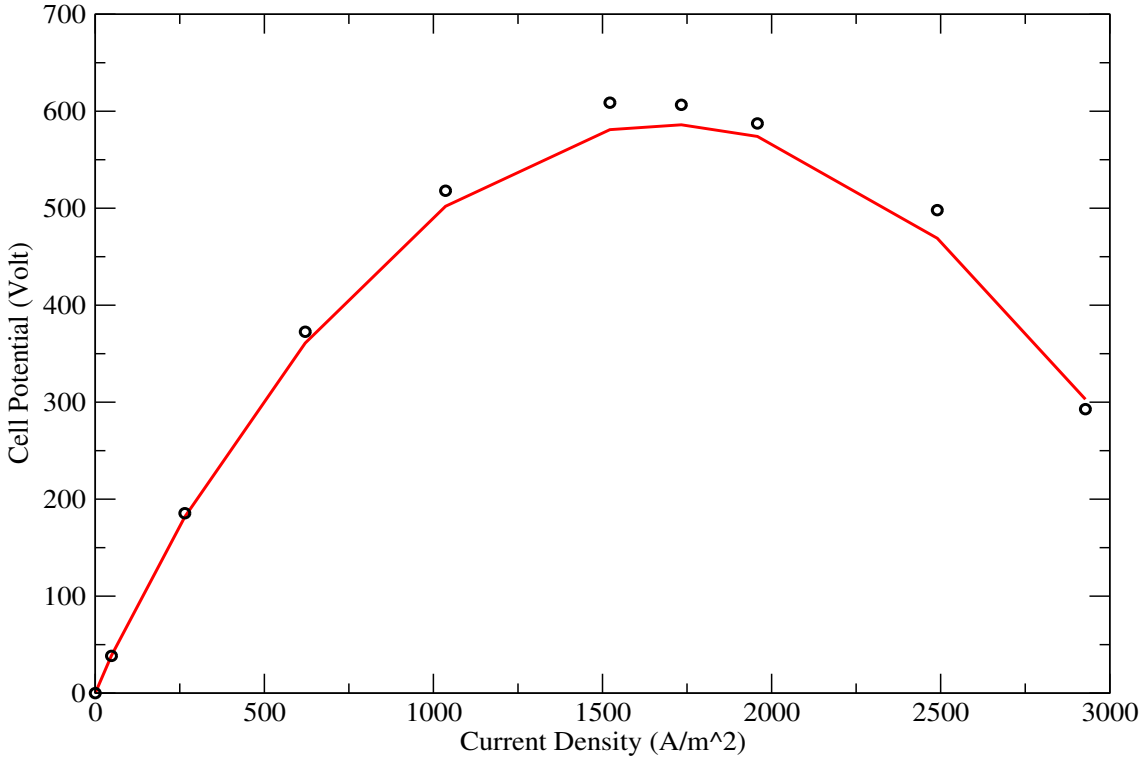

Figure 11: Power Density curve.

at the membrane and allows a significant simplification of the numerical procedure to solve the transport equations in the cell. The chose of Ochoa's porous media models avoids the need of matching conditions at the channels-GDL interfaces. A simple an efficient iterative algorithm is depicted. The model was implemented in a developed module attached to OpenFoam general package. Results are physically consistent and comparisons show a very good agreement with available in-house experimental data.

7. Aknowledgements

The authors want to aknowledge the Spanish Ministry of Science and Innovation fot its support trhough grant ENE2011-29731-C05-01

References

[1] T. Springer, T. Zawodzinski, S. Gottesfeld, Modelling of bateries and fuel cells, in: R.e. white, m.w. verbrugge, j.f. stockel (eds.), in: The electrochemestry Society Softbound Proceedings Series, Pennington, NJ, 1991, p. 209.

[2] D. Bernardi, W. Verbrugge, Mathematical model of a gas diffusion electrode bounded to a polymer electrolyte, AIChE Journal 37 (1991) 1151–1163.

[3] D. Bernardi, W. Verbrugge, A mathematical model of the solidpolymerelectrolyte fuel cell, Journal of The Electrochemical Society 139 (1992) 2477–2491.

[4] V. Gurau, H. Liu, S. Kakac, Two-dimensional model for proton exchange membrane fuel cell, AIChE Journal 44 (11) (1998) 2410–2422.

[5] D. Singh, D. Lu, N. Djilali, 3-d computational analysis of transport phenomena in a pem fuel cell, Int. J. Eng. Sci. 37 (1999) 431–452.

[6] T. Nguyen, R. White, A water and heat management model for protonexchangemembrane fuel cells, Journal of The Electrochemical Society 140 (1-2) (1993) 2178–2186.

[7] S. Dutta, S. Shimpalee, J. V. Zee, Three dimensional numerical simulation of straight channel pem fuel cells, Journal Appl. Electrochem (1999) 135–146.

[8] T. Berning, D. Lu, N. Djilali, 3-d computational analysis of transport phenomena in a pem fuel cell, Journal of Power Sources 106 (1-2) (2002) 284–294.

[9] T. Zhou, H. Liu, A general three-dimensional model for proton exchange membrane fuel cell, International Journal of Transport Phenomena 3 (2001) 177–198.

[10] Y. Wang, J. Mishler, Modeling and analysis of polymer electrolyte fuel cell cold-start, ASME 2010 4th International Conference on Energy Sustainability, ES 2010 1 (2010) 201–206.

[11] R. Mustata, L. Valiño, F. Barreras, M. Gil, A. Lozano, Study of the distribution of air flow in a proton exchange membrane fuel cell stack, Journal of Power Sources 192 (2009) 185–189.

[12] J. Sierra, J. Moreira, P. Sebastian, Numerical analysis of the effect of different gas feeding modes in a proton exchange membrane fuel cell with serpentine flow-field, Journal of Power Sources 196 (11) (2011) 5070–5076.

[13] M. Coppo, N. Siegel, M. von Spakovsky, On the influence of temperature on pem fuel cell operation, Journal of Power Sources 159 (1) (2006) 560 – 569.

[14] A. Arvay, A. Ahmed, X.-H. Peng, A. Kanna, Convergence criteria establishment for 3d simulation of proton exchange membrane fuel cell, International Journal of Hydrogen Energy 37 (3) (2012) 2482 – 2489.

[15] P. Alotto, M. Guarnieri, F. Moro, A. Stella, Multi-physic 3d dynamic modelling of polymer membranes with a proper generalized decomposition model reduction approach, Electrochimica Acta 57 (0) (2011) 250 – 256.

[16] E. Ubong, Z. Shi, X. Wang, Three-dimensional modeling and experimental study of a high temperature pbi-based pem fuel cell, Journal of the Electrochemical Society 156 (10) (1991) B1276–B1282.

[17] L. Onsager, Reciprocal relations in irreversibles processes. ii., Physical Review 38 (12) (1931) 2265–2279.

[18] J. A. Ochoa-Tapia, S. Whitaker, Momentum transfer at the boundary between a porous medium and a homogeneous fluid–I. Theoretical development, International Journal of Heat and Mass Transfer 38 (14) (1995) 2635–2646.

[19] J. A. Ochoa-Tapia, S. Whitaker, Momentum transfer at the boundary between a porous medium and a homeogenos fluid-ii. comparison with experiment, International Journal of Heat and Mass Transfer 38 (14) (1995) 2647–2655.

[20] Z. Fishman, A. Bazylak, Heterogeneous through-plane distributions of tortuosity, effective diffusivity, and permeability for pemfc gdls, Journal of The Electrochemical Society 158 (2) (2011) B247–B252.